Evaluation of internal potential distribution and carrier extraction properties of organic solar cells through Kelvin probe and time-of-flight measurements

Yuya Tanaka, Yutaka Noguchi' , Keisuke Oda, Yasuo Nakayama, Jun-ichi Takahashi, Hiroshi Tokairin, and Hisao Ishii'

Citation: J. Appl. Phys. **116**, 114503 (2014); doi: 10.1063/1.4895712
View online: http://dx.doi.org/10.1063/1.4895712
View Table of Contents: http://aip.scitation.org/toc/jap/116/11
Published by the American Institute of Physics

Evaluation of internal potential distribution and carrier extraction properties of organic solar cells through Kelvin probe and time-of-flight measurements

Yuya Tanaka,[1] Yutaka Noguchi,[1,2,a)] Keisuke Oda,[1] Yasuo Nakayama,[1] Jun-ichi Takahashi,[3] Hiroshi Tokairin,[3] and Hisao Ishii[1,2,b)]
[1]*Graduate School of Advanced Integration Science, Chiba University, Chiba 263-8522, Japan*
[2]*Center for Frontier Science, Chiba University, Chiba 263-8522, Japan*
[3]*Advanced Technology Research Laboratories, Idemitsu Kosan Co., Ltd. Sodegaura 299-0293, Japan*

(Received 7 May 2014; accepted 3 September 2014; published online 16 September 2014)

The carrier extraction property of a prototypical small molecule organic solar cell (OSC) composed of copper phthalocyanine (CuPc), C_{60}, and bathocuproine (BCP) was studied on the basis of the internal potential distribution and carrier dynamics in the device. The internal potential distribution in the OSC structure at the interfaces and in the bulk region was determined by the Kelvin probe method. Significant potential gradients were found in the CuPc film on indium tin oxide and in the C_{60} film on CuPc, consistent with charge transfer through the contacts. Moreover, surface potential of the BCP layer grew linearly with increasing film thickness with a slope of *ca.* 35 mV/nm (giant surface potential: GSP), which indicated spontaneous orientation polarization in the film. The potential gradient and GSP significantly changed the built-in potential of the device. Current–voltage and modified time-of-flight measurements revealed that the BCP layer worked as an electron injection and extraction layer despite the wide energy gap. These results were discussed based on the contributions of GSP and the gap states in the BCP layer. © *2014 AIP Publishing LLC*. [http://dx.doi.org/10.1063/1.4895712]

I. INTRODUCTION

Organic solar cells (OSCs) have been extensively studied toward practical use[1–3] since Tang invented a planar heterojunction OSC with a high power conversion efficiency (η) of 0.95%.[4] Advanced device structures such as p-type–intrinsic–n-type (p–i–n) layers,[5,6] bulk-heterojunction,[7,8] and tandem cell structures[9,10] have been developed to improve η. In addition, the insertion of additional layers between the electrode and organic layer has further improved device efficiency and lifetime.

Peumans *et al.* observed a considerable increase in planar heterojunction OSC performances by inserting a thin bathocuproine (BCP) layer between C_{60} acceptor and Al cathode.[11,12] Subsequent studies[13–17] conducted to understand the roles of the BCP layer revealed that this layer acts as (i) an exciton blocking layer prohibiting exciton diffusion to the cathode, (ii) a buffer layer restricting the diffusion of cathode materials into the acceptor layer, and (iii) an electron injection-extraction layer reducing the contact resistance. Although the first two roles are easily acceptable, the third one appears incongruous because BCP is a wide gap material and interfaces are expected to present a high energy barrier for electron injection and extraction. These previous results suggest that a simple energy diagram is insufficient to explain the carrier dynamics resulting from the BCP layer.

Previous reports have suggested that electron transport through the BCP layer stemmed from "gap states" formed in the highest occupied molecular orbital–lowest unoccupied molecular orbital (HOMO–LUMO) gap of BCP.[12,17] Although their nature in organic semiconductors remains unsolved, gap states are believed to play a key role in carrier dynamics at the interface. Ultra high sensitivity measurements by Nakayama *et al.* have recently detected their presence at the interface of BCP on C_{60} film using low energy-ultraviolet photoelectron spectroscopy (LE-UPS).[18] Weak density of states was observed around the Fermi level of the Al cathode, which may provide a charge transport path even in the wide gap material.

Another notable feature of BCP is giant surface potential (GSP) in the evaporated film originating from the slight orientational order of permanent dipole moment in the amorphous film. GSP was discovered in a tris-(8-hydroxyquinolinate) aluminum (Alq_3) film evaporated on a gold substrate.[19] In this Alq_3 film, the surface potential (SP) grew linearly as a function of film thickness with a slope of 50 mV/nm to reach 28 V at 560 nm. Two years earlier than this publication, Berleb *et al.* revealed the presence of negative interface charge at *N*,*N*′-diphenyl-*N*,*N*′-bis(1-naphtyl)–1,1′-biphenyl-4,4′-diamine (NPB)/Alq_3 interface in a typical organic light-emitting diode, though the origin remained unclear.[20] Recently, Noguchi *et al.* reported that the negative interface charge originates from the polarization charge due to GSP, i.e., orientation polarization of the evaporated films.[21,22] Several polar molecules including not only Alq_3 but also BCP show the GSP behavior in the evaporated film and it remains in the actual devices.[22] The GSP slope of the BCP film formed on a 4,4′-bis[*N*–(1-naphthyl)–*N*-phenylamino]-biphenyl (α-NPD) film was 33 mV/nm. Consequently, the GSP-induced built-in potential exceeds a few hundreds

a)Present address: School of Science and Technology, Meiji University, Kawasaki 214-8571, Japan. Electronic address: noguchi@meiji.ac.jp
b)Electronic address: ishii130@faculty.chiba-u.jp

millivolts at typical film thicknesses found in actual devices (>10 nm) and changes the carrier dynamics in the resulting devices.

Because of these specific features of the BCP layer, a detailed investigation of carrier dynamics based on the potential distribution in actual device structures is required. In this study, the internal potential distribution of prototypical OSC model structures at the interface and in the bulk region (up to 100 nm) was evaluated by the Kelvin probe (KP) method. The BCP on C_{60} film displayed a GSP with a slope of *ca.* 35 mV/nm, drastically changing the internal potential in the resulting OSC. In addition, carrier extraction properties of actual devices were examined through a modified time-of-flight (TOF) measurement, which facilitates the evaluation of carrier blocking at organic heterointerfaces.[23] The TOF measurement revealed that the energy barrier at the C_{60}/BCP interface significantly delayed the hole extraction from the C_{60} layer to the Al electrode through the BCP layer, while the electron extraction occurred smoothly. Moreover, current–voltage (*I–V*) characteristics showed that the insertion of BCP layer enhanced the current density and η to a large extent. These results are explained by considering the electron transport through the gap states assisted by GSP of the BCP layer.

II. EXPERIMENTAL

SP measurements were performed using a KP in a high vacuum system with a base pressure of 4×10^{-4} Pa. Sample structures consisted of CuPc (junction A), BCP on C_{60} (junction B), and BCP on C_{60} on CuPc (junction C) [Fig. 1(a)]. All samples used indium-tin-oxide (ITO) coated glass substrates. The organic films were incrementally formed at a typical deposition rate of 0.5–1.0 Å/s, and SP measurements were conducted *in situ* at each step of the deposition using the work function of ITO as a reference. SP variations were measured in each layer up to 100 nm in junctions A and B to determine the saturation property of SP. Junction C is an OSC model structure in which each layer thickness corresponds to those in prototypical OSC. The responsiveness to the light of SP in junction C was evaluated by irradiation from a halogen lamp though a glass viewport without any filter. Because GSP is likely to decay upon light absorption of the film,[19,24,25] all the above procedures except the photoresponse measurements were performed in the dark.

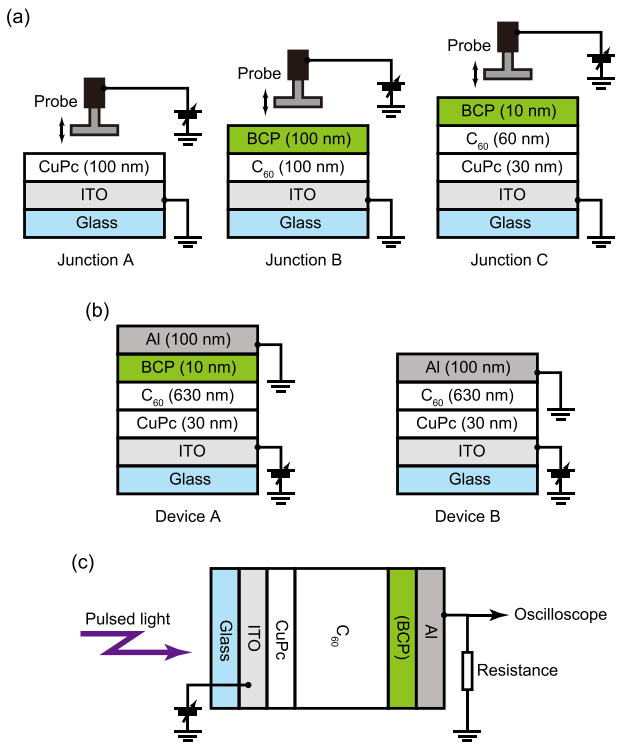

FIG. 1. (a) Schematics of the sample structures for KP measurements. (b) Schematic of the device structures for the *I–V* and TOF measurements. (c) A measurement setup for TOF measurement.

TOF and *I–V* measurements were performed in device A, which was composed of ITO/CuPc (30 nm)/C_{60} (630 nm)/BCP (10 nm)/Al (100 nm), and device B, a control device that displayed the same structure without the BCP layer [Fig. 1(b)]. Note here that the C_{60} layer was much thicker in these devices than in the optimized OSC prototype, in order to examine carrier propagation and extraction processes. The devices were encapsulated in a N_2-filled glove box to prevent air exposure.

TOF measurements were performed using a N_2 pulsed laser (wavelength: 337.1 nm, pulse width: 600 ps) as a light source to generate transient photocarriers [Fig. 1(c)]. The bias voltage was applied to ITO using the Al cathode as a reference. The transient photocurrent was measured under air mass (AM) 1.5 G simulated sunlight illumination using a digital oscilloscope through a 100 Ω sensor resistor.

III. RESULTS

A. Kelvin probe measurements

Figure 2(a) shows SP variations in junction A as a function of CuPc thickness. Here, the downward shift is defined as the positive change in SP, corresponding to the direction of the vacuum level shift. When the thickness increased to 1 nm, SP shifted downward by 80 mV [inset of Fig. 2(a)] as a result of interface dipole formation.[26] Subsequently, SP linearly increased with a slope of 32 mV/nm when the thickness increased up to 20 nm. This growth gradually slowed down upon further deposition of CuPc, but SP did not reach full saturation within a thickness of 100 nm. Note here that the linear growth does not correspond to GSP, because CuPc is a nonpolar molecule. The details will be discussed in Sec. IV A.

The open triangles in Fig. 2(b) show SP variations in the C_{60} film on ITO. SP decreased rapidly at the initial deposition stage, indicating the formation of the interface dipole [upper inset, Fig. 2(b)]. After this shift, SP of the C_{60} layer remained almost constant at around −0.07 V in the entire thickness region. SP variations in junction B were also shown as a function of thickness upon BCP film deposition on the C_{60} layer [open squares, Fig. 2(b)]. A downward shift of SP was observed at the BCP on C_{60} interface within a thickness of 1 nm [lower inset, Fig. 2(b)]. This shift was followed by a clear GSP behavior, which extended over a wide thickness range (5–100 nm) with a mean slope of 37 mV/nm. This result suggests that spontaneous orientation polarization occurs in the BCP layer of actual devices.

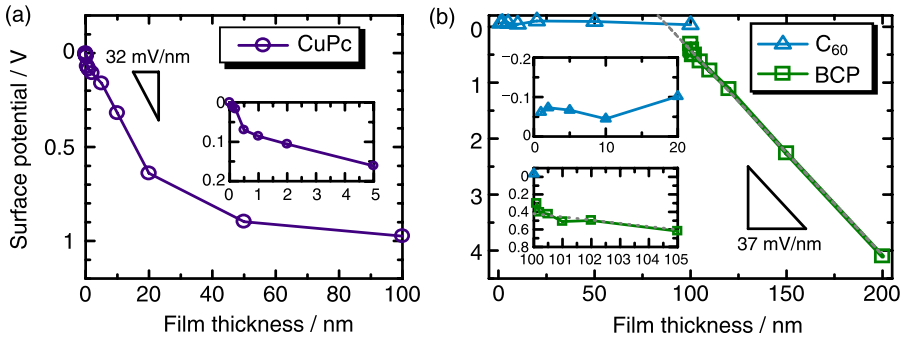

FIG. 2. (a) Variation in surface potential of junction A as a function of CuPc thickness. Surface potential is plotted with reference to that of ITO. Inset shows the expansion of the interface region. (b) Variation in surface potential of junction B as a function of film thickness. Insets show expansions of the interface regions of C_{60} on ITO (top) and BCP on C_{60} (bottom).

Figure 3(a) shows the SP profile of junction C, along with the SP behavior at the heterointerfaces (I–III). In the CuPc layer, SP grew almost linearly within the measured thickness region [inset I, Fig. 3(a)]. The SP of C_{60} on the CuPc layer [inset II, Fig. 3(a)] dropped by 0.43 V upon interface formation before decreasing slowly to saturation upon further deposition of C_{60}. Upon deposition of BCP on the C_{60} layer, SP exhibited a nonlinear growth in the interface region, followed by a GSP region with a slope of 33 mV/nm [open squares, Fig. 3(a)].

Figure 3(b) shows SP variations under light illumination. In the dark, SP was estimated to be *ca.* 0.84 V. Under light irradiation, SP decreased within 10 s to reach a saturation value of 0.54 V, indicating that junction C worked as a model system for an operating solar cell. The photoinduced voltage was estimated to be *ca.* 0.3 V, which is close to the typical open circuit voltage for CuPc/C_{60}-based OSCs.[1] SP was almost fully recovered in the dark after light irradiation, indicating that the GSP decay did not occur in the BCP layer of this junction.

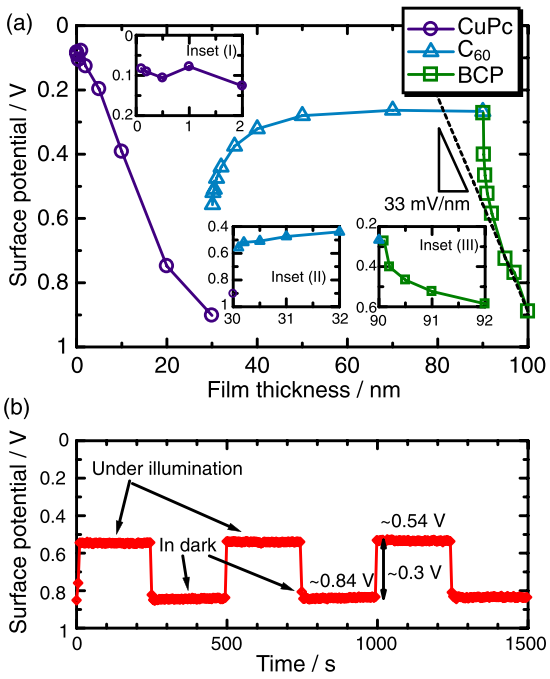

FIG. 3. (a) Surface potential of junction C as a function of film thickness. Insets (I), (II), and (III) indicate the expansions of the interface regions at CuPc on ITO, C_{60} on ITO, and BCP on C_{60} interfaces, respectively. (b) Photoresponse of surface potential induced by the light illumination.

Figure 4 depicts the energy diagram of junction C based on KP results assuming a work function of 4.8 eV for ITO; CuPc LUMO and HOMO energies of 3.2 and 4.86 eV; C_{60} LUMO and HOMO energies of 4.1 and 6.4 eV; and BCP LUMO and HOMO energies of 1.6 and 6.3 eV, respectively.[18,27,28] The energy diagram is consistent with previous reports.[18,29,30] Hole extraction from the CuPc layer to ITO anode is expected to be enhanced because of the favorable potential gradient in the CuPc layer. On the other hand, C_{60}/BCP and BCP/Al interfaces displayed energy barriers for holes and electrons. These energy barriers seem to increase the contact resistance at the cathode side, although they efficiently prohibit the exciton diffusion towards the cathode where they would otherwise be quenched.[17]

B. Current voltage and time-of-flight measurements

Figures 5(a) and 5(b) show the *I–V* curves of devices A and B, respectively. The power conversion efficiencies of devices A and B amounted to 0.13% and 0.07%, respectively, under AM 1.5 G simulated sunlight illumination. The *I–V* curves under the dark show considerable leakage at the negative biases, indicating a low shunt resistance of these devices. Moreover, the *I–V* curve of device B under illumination significantly depended on voltage below the open circuit voltage, suggesting a high contact resistance at the C_{60}/Al interface.[14,37,38]

The TOF curves of devices A and B were evaluated at a forward bias of 2.0 V under the simulated sunlight illumination for short [1×10^{-8} to 9×10^{-6} s, Fig. 6(a)] and long-

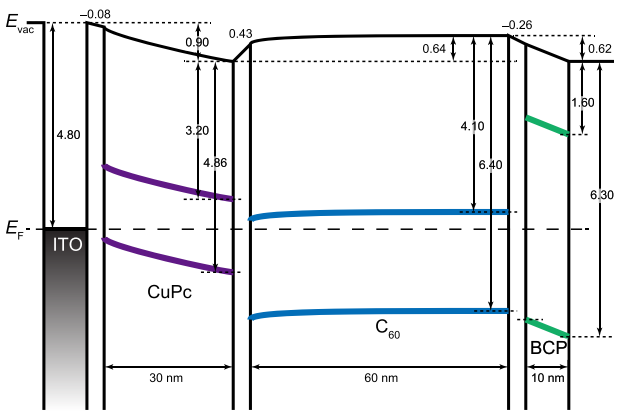

FIG. 4. An energy diagram of the organic solar cell based on the KP results. The ordinate corresponds to the energy in eV with reference to the vacuum level and the abscissa is the thickness (*d*) of the organics.

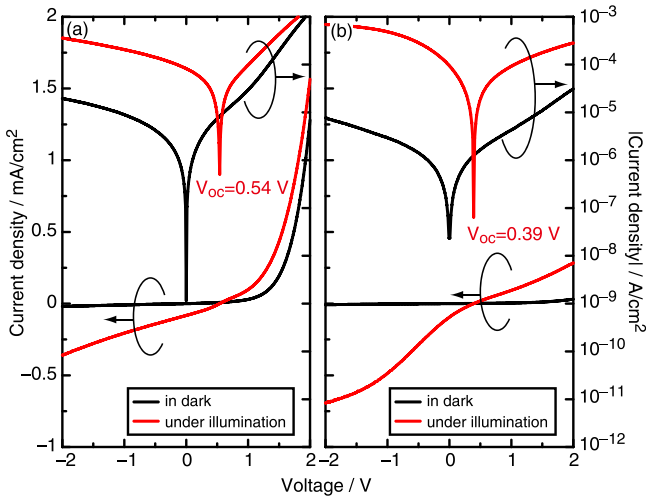

FIG. 5. (a) *I–V* curves in dark and under illumination of device A (with BCP layer). $V_{oc} = 0.54\,\mathrm{V}$, $J_{sc} = -0.082\,\mathrm{mA/cm^2}$, $FF = 0.29$, $\eta = 0.13$. (b) *I–V* curves of device B (without BCP layer). $V_{oc} = 0.39\,\mathrm{V}$, $J_{sc} = -0.097\,\mathrm{mA/cm^2}$, $FF = 0.19$, $\eta = 0.07$.

time scales [1×10^{-6} to 9×10^{-4} s, Fig. 6(b)]. In addition, corresponding curves were determined at a reverse bias of –2.0 V for the same short [Fig. 6(c)] and long time scales [Fig. 6(d)]. The horizontal dashed lines in Figs. 6(a)–6(d) indicate the background level of our system (0.2 mA/cm^2).

The photocarriers were mainly generated near the ITO electrode at time zero, propagated through the device, and were finally swept out from the device because of the external electric field. Therefore, the carrier extraction time (τ) was assumed to be the time spent for the photocurrent to decay to the background level. Here, carrier extraction times at a certain biasing voltage V were referred to $\tau_A(V)$ and $\tau_B(V)$ for devices A and B, respectively. The intersection of the linear approximation curve of the current (dotted lines) and the background level in the log–log plot gave hole extraction times $\tau_A(2.0)$ and $\tau_B(2.0)$ of 2.1×10^{-5} s and 3.9×10^{-6} s, respectively. Similarly, the electron extraction times $\tau_A(-2.0)$ and $\tau_B(-2.0)$ were determined to be 5.9×10^{-5} s and 3.8×10^{-5} s, respectively. Here, the extraction time for holes is shorter than for electrons, suggesting that the holes are smoothly extracted rather than the electrons, although C_{60} is commonly considered as electron transporter. This result implies that the intensity of the internal electric field in these devices is different depending on the bias polarity, e.g., due to the built-in potential as shown in Fig. 4 and the charge accumulation at the C_{60}/(BCP)/Al interfaces.

The current decay of device B at early times of the transient [Figs. 6(a) and 6(c)] is faster than that of device A. A possible explanation is the difference of the internal potential distribution in these devices. A weak electric field is expected in the C_{60} layer of device A at the forward bias because of the hole accumulation at the C_{60}/BCP interface, resulting in the slow decay of photo-generated current. At the negative bias, the electron accumulation is not significant as discussed later, but the potential drop due to GSP in the BCP layer may reduce the electric field in the C_{60} layer.

IV. DISCUSSION

A. Potential distribution in the model structures

The CuPc film on ITO exhibited significant thickness-dependent potential changes [Figs. 2(a) and 3(a)], which extended to an unexpected thick region (~100 nm). The direction of this SP change indicates a positive charge transfer from ITO to CuPc. The excess positive charges may be retained at finite densities of states in the HOMO-LUMO gap (gap states) in the CuPc film. Recently, Nakayama *et al.* have directly detected these gap states above the HOMO level of the CuPc film on the ITO substrate by LE-UPS.[18] At the system's Fermi level, the photoelectron signal from the occupied gap states (n_{gap}) of a 30-nm-thick CuPc film remains in approximately 1/500 of the signal from the HOMO peak (n_{peak}).

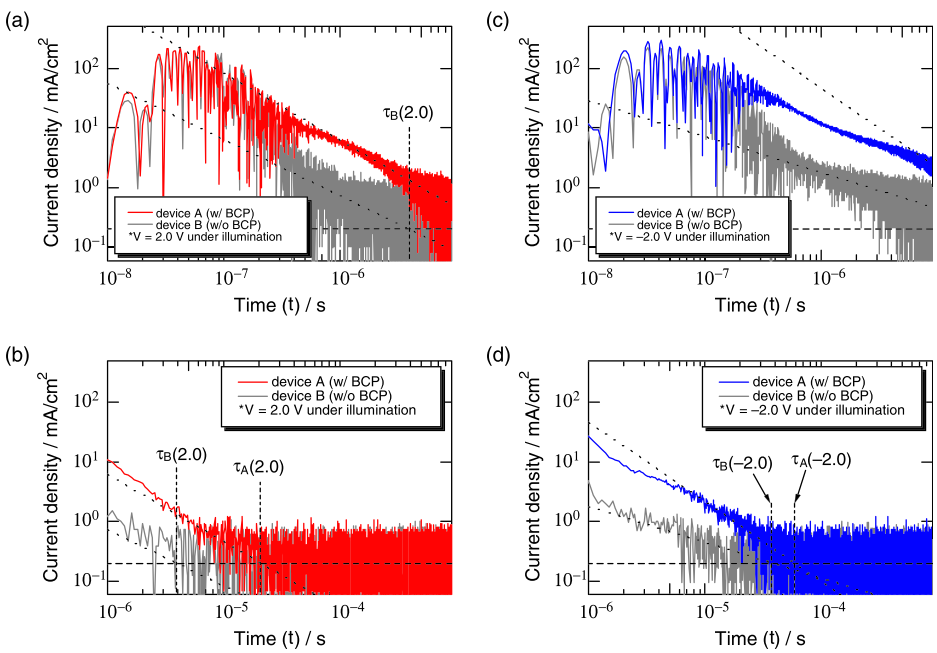

FIG. 6. Log-log plot of the transient current vs. time curves of device A and device B at $V = 2.0$ V under illumination in (a) a short-time scale (1×10^{-8}–9×10^{-6} s) and (b) a long-time scale (1×10^{-6}–9×10^{-4} s). Those at $V = -2.0$ V in (c) a short-time scale and (d) a long-time scale. $\tau_A(V)$ and $\tau_B(V)$ indicate the time when at the applied voltages of V, all of the photo-generated carriers are discharged from device A and device B, respectively.

Here, the excess charge density in the 30-nm-thick CuPc film was estimated approximately. The surface potential of the CuPc film is almost proportional to the film thickness in this region. According to the Poisson's law, the linear growth of the film potential indicates the absence of excess charges in the bulk of the film. Therefore, excess charges were assumed to exist only on the film surface, and the density is given by $\sigma = \epsilon V/d$, where σ is the charge density per unit area, ϵ is the dielectric permittivity of the CuPc film, and V/d is the potential gradient. Consequently, σ was estimated to be 0.96 mC/m^2 by assuming a relative dielectric constant of 3.4 (Ref. 31) and a potential gradient of 32 V/nm for the CuPc film. The excess charge density corresponded to approximately one positive charge per more than two hundreds molecules on the surface. Here, the density of the CuPc film was assumed to be 1.6 g/cm^3.[32] The portion of positively charged molecules is close to the experimentally determined n_{gap}/n_{peak} ratio. Note here that UPS detects the photoelectrons from the occupied states but the ratio of unoccupied gap states should be similar to n_{gap}/n_{peak} ratio, because the density of states is half-filled at the Fermi level. Furthermore, our result suggests that the gap states extend over distance exceeding 100 nm from the CuPc on ITO interface. Although their origin is not fully understood, gap states at the CuPc on ITO interface and in the bulk may result from structural imperfectness of the film.[18,33,34]

The C_{60} film displayed an upward band bending when deposited on CuPc but not on ITO. Because the CuPc layer shows a downward potential shift on ITO, its work function is expected to be lower than that for the C_{60} film, resulting in electron transfer from CuPc to C_{60} at the contact and upward band bending in the C_{60} layer, which accelerate the hole velocity and decelerate the electron velocity. Because the energy gap between HOMO of CuPc and LUMO of C_{60} is expected to be much higher than the thermal energy (Fig. 4), the gap states at the interface may mediate the electron transfer.[35]

The BCP on C_{60} film clearly showed a positive GSP behavior, indicating the presence of polarization charges of opposite polarity at the top and bottom of the film. A positive GSP results in a negative interface charge at the bottom side interface, which is the BCP on C_{60} interface in our sample structure. The density of this negative interface charge should be $-\epsilon V/d$ C/m^2. At the BCP on C_{60} interface, this density amounted to -1.0 mC/m^2, assuming a relative dielectric constant of 3.4 for the BCP film.[22] In OSCs containing a BCP layer, holes are likely to accumulate at the interface until they compensate the negative interface charge under forward biases.[22,36] However, under reverse bias, GSP induces excess electric field in the BCP layer. This electric field may support electron extraction from the device to the cathode.

The surface potential of junction C decreased by 0.3 V under light illumination, but almost completely recovered after the light was switched off. In the case of Alq_3 films, GSP decayed irreversibly upon light absorption because photocarriers in the film accumulated at the film surface to cancel GSP.[19,24,25] Our result suggests an inefficient generation of photocarriers in the BCP layer compared to Alq_3. On the other hand, the SP of junction C before BCP deposition was 0.3 V [Fig. 3(a)], which is in agreement with the photoinduced change. This result implies that light illumination produced a flat band condition in junction C, except in the BCP layer. In other words, the photocarriers in the C_{60} film did not penetrate into the BCP layer, although the GSP-induced electric field remained in this layer. To understand the role of the BCP layer, carrier dynamics should be studied in the actual device.

B. Role of the BCP layer in organic solar cells

The *I–V* curve of device A showed a diode behavior, and the rectification ratio at ± 2 V, defined as $I(+2)/I(-2)$, was calculated to be 65. On the other hand, device B displayed a much lower current density under forward bias than device A, and its rectification ratio was only 4. In addition, the *I–V* curve of device B under illumination showed an "S-shape."[37,38] The low rectification ratio and the S-shaped *I–V* curve suggest a poor electron injection property at the C_{60}/Al interface despite the low energy barrier although the considerable leakage also plays a role in the low rectification ratio.

As described previously, the energy barriers for electrons and holes are formed upon insertion of the BCP layer, which is consistent with the energy diagram (Fig. 4). These energy barriers are expected to restrict the carrier injection–extraction between the C_{60} layer and the Al cathode. Nevertheless, device A exhibits higher efficiency and rectification ratio than device B. These results suggest that the BCP layer works as an electron injection–extraction layer in device A to reduce the contact resistance. Here, this BCP layer is unlikely to act as an exciton blocking layer because the C_{60} layer is much thicker than the exciton diffusion length ($\sim$40 nm).[1]

As shown in Fig. 6(b), the time required to discharge the photogenerated holes was about 10 times longer in device A [$\tau_A(2.0)$] than that in device B [$\tau_B(2.0)$]. Here, two hole blocking mechanisms should be considered at the C_{60}/BCP interface, the negative interface charge and the energy barrier.[39] A part of transported holes are captured at the C_{60}/BCP interface by the negative interface charge until charge compensation. However, this hole blocking mechanism is invalid for the amount of holes more than that of the interface charge. Under forward biases ($\geq V_{oc}$), the negative interface charge at C_{60}/BCP interface is expected to be canceled by accumulation of the photogenerated and injected holes [Fig. 7(a)]. Thus, the delayed extraction of holes from device A is likely to originate from the energy barrier at the C_{60}/BCP interface, as expected from the energy diagram.

On the other hand, the extraction time for electrons at a reverse bias of device A [$\tau_A(-2.0)$] is similar to that of device B [$\tau_B(-2.0)$] as shown in Fig. 6(d), indicating that the electrons are discharged smoothly in both devices notwithstanding the high energy barrier for electrons expected in device A (Fig. 4). This result is consistent with impedance spectroscopy measurements, which exhibited a low resistivity of the BCP layer in OSC.[40] It has been suggested that the gap states were formed within the HOMO-LUMO gap of BCP and they serve a path to the electron transport.[1] The

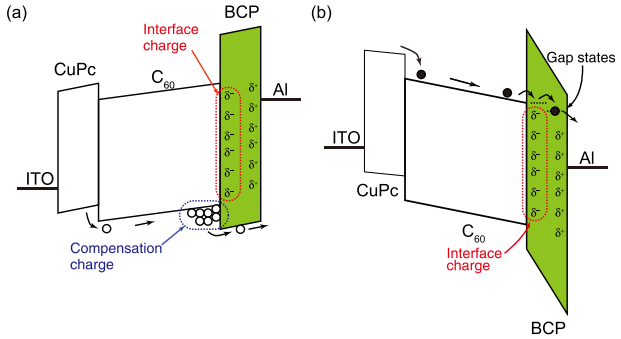

FIG. 7. Schematic illustrations of energy diagram at (a) the forward applied bias and (b) backward bias. Holes and electrons are expressed by open and filled circles, respectively.

presence of the gap states was recently confirmed, and the gap states of BCP were indeed observed near the Fermi level of Al (~4 eV) and thus provide a path for the electron extraction [Fig. 7(b)].[18]

Another possible factor for improving electron extraction is the electric field owing to GSP, which is formed as a favorable direction to extract the electrons from the device. Since there are no holes to compensate the negative interface charge at the reverse bias, the electric field of GSP can work for the electron extraction. On the other hand, GSP may also improve the electron injection property at the forward biases because of the positive polarization charge at the BCP/Al interface. This may induce the electron injection from the cathode.[41,42] Actually, some positive GSP materials are used underneath the cathode as the electron injection layer in organic light-emitting diodes, including Alq_3 and 1,3,5-tris(1-phenyl-1 H-benzimidazol-2-yl)benzene (TPBi). In addition, a high performance of OSC using Alq_3 or TPBi instead of BCP has been reported.[43,44] GSP materials have been unintentionally used in the organic devices; however, GSP possibly contributes to improve the device performance.

V. CONCLUSION

In summary, the potential distribution of OSC model structures was investigated not only at the interface but also in the bulk region by the KP method. We found significant potential gradient in the CuPc film on ITO and C_{60} film on CuPc, as well as GSP in the BCP film. The role of the BCP layer was examined by a modified TOF method and *I–V* measurement. Even though a high energy barrier for both electrons and holes is expected at the C_{60}/BCP interface, the electron extraction time was comparable to that of the device without the BCP layer, while holes were well blocked at the interface. Moreover, the *I–V* curves suggest that the BCP layer enhances electron injection from Al. These properties are explained by considering GSP as well as the gap state of the BCP layer, although further investigation is needed to explore the causal relationship between GSP and the efficiency of OSCs.

ACKNOWLEDGMENTS

This study was supported by JSPS through the "Funding Program for World-Leading Innovative R&D on Science and Technology (FIRST Program)" initiated by the Council for Science and Technology Policy, the Global-COE program at Chiba University (Advanced School for Organic Electronics, G-03, MEXT), KAKENHI (Grant No. 21245042), and the New Energy and Industrial Technology Development Organization (NEDO). Y.T. gratefully acknowledges JSPS Research Fellowships for Young Scientists (Grant No. 22·7042).

[1]P. Peumans, A. Yakimov, and S. R. Forrest, J. Appl. Phys. **93**, 3693 (2003).
[2]A. W. Hains, Z. Liang, M. A. Woodhouse, and B. A. Gregg, Chem. Rev. **110**, 6689 (2010).
[3]M. Jørgensen, K. Norrman, S. A. Gevorgyan, T. Tromholt, B. Andreasen, and F. C. Krebs, Adv. Mater. **24**, 580 (2012).
[4]C. W. Tang, Appl. Phys. Lett. **48**, 183 (1986).
[5]M. Hiramoto, H. Fukusumi, and M. Yokoyama, Appl. Phys. Lett. **58**, 1062 (1991).
[6]J. Xue, B. P. Rand, S. Uchida, and S. R. Forrest, Adv. Mater. **17**, 66 (2005).
[7]G. Yu, J. Gao, J. C. Hummelen, F. Wudl, and A. J. Heeger, Science **270**, 1789 (1995).
[8]J. J. M. Halls, C. A. Walsh, N. C. Greenham, E. A. Marseglla, R. H. Friend, S. C. Moratti, and A. B. Holmes, Nature **376**, 498 (1995).
[9]J. Xue, S. Uchida, B. P. Rand, and S. R. Forrest, Appl. Phys. Lett. **85**, 5757 (2004).
[10]B. Yu, F. Zhu, H. Wang, G. Li, and D. Yan, J. Appl. Phys. **104**, 114503 (2008).
[11]P. Peumans, V. Bulovic, and S. R. Forrest, Appl. Phys. Lett. **76**, 2650 (2000).
[12]P. Peumans and S. R. Forrest, Appl. Phys. Lett. **79**, 126 (2001).
[13]Z. R. Hong, Z. H. Huang, and X. T. Zeng, Chem. Phys. Lett. **425**, 62 (2006).
[14]M. Vogel, S. Doka, Ch. Breyer, M. Ch Lux-Steiner, and K. Fostiropoulos, Appl. Phys. Lett. **89**, 163501 (2006).
[15]Z. R. Hong, Z. H. Huang, and X. T. Zeng, Thin Solid Films **515**, 3019 (2007).
[16]Q. L. Song, C. M. Li, M. L. Wang, X. Y. Sun, and X. Y. Hou, Appl. Phys. Lett. **90**, 071109 (2007).
[17]H. Gommans, B. Verreet, B. P. Rand, R. Muller, J. Poortmans, P. Heremans, and J. Genoe, Adv. Funct. Mater. **18**, 3686 (2008).
[18]Y. Nakayama, T. L. Nguyen, Y. Ozawa, S. Machida, T. Sato, H. Tokairin, Y. Noguchi, and H. Ishii, Adv. Energy Mater. **4**, 1301354 (2014).
[19]E. Ito, Y. Washizu, N. Hayashi, H. Ishii, N. Matsuie, K. Tsuboi, Y. Ouchi, Y. Harima, K. Yamashita, and K. Seki, J. Appl. Phys. **92**, 7306 (2002).
[20]S. Berleb, W. Brütting, and G. Paasch, Org. Electron. **1**, 41 (2000).
[21]Y. Noguchi, N. Sato, Y. Tanaka, Y. Nakayama, and H. Ishii, Appl. Phys. Lett. **92**, 203306 (2008).
[22]Y. Noguchi, Y. Miyazaki, Y. Tanaka, N. Sato, Y. Nakayama, T. D. Schmidt, W. Brütting, and H. Ishii, J. Appl. Phys. **111**, 114508 (2012).
[23]M. M. Rahman, N. Ogawa, Y. Miyazaki, Y. Nakayama, Y. Noguchi, and H. Ishii, e-J. Surf. Sci. Nanotechnol. **10**, 315 (2012).
[24]K. Yoshizaki, T. Manaka, and M. Iwamoto, J. Appl. Phys. **97**, 023703 (2005).
[25]K. Ozasa, H. Ito, M. Maeda, and M. Hara, Appl. Phys. Lett. **98**, 013301 (2011).
[26]H. Ishii, K. Sugiyama, E. Ito, and K. Seki, Adv. Mater. **11**, 605 (1999).
[27]J. X. Tang, Y. C. Zhou, Z. T. Liu, C. S. Lee, and S. T. Lee, Appl. Phys. Lett. **93**, 043512 (2008).
[28]N. Li, B. E. Lassiter, R. R. Lunt, G. Wei, and S. R. Forrest, Appl. Phys. Lett. **94**, 023307 (2009).
[29]K. Akaike, K. Kanai, Y. Ouchi, and K. Seki, Adv. Funct. Mater. **20**, 715 (2010).
[30]K. Akaike and Y. Kubozono, Org. Electron. **14**, 1 (2013).
[31]S. Zhong, J. Q. Zhong, H. Y. Mao, J. L. Zhang, J. D. Lin, and W. Chen, Phys. Chem. Chem. Phys. **14**, 14127 (2012).
[32]K. W. Hipps and J. J. Hoagland, Langmuir **7**, 2180 (1991).
[33]H. Yamane, Y. Yabuuchi, H. Fukagawa, S. Kera, K. K. Okudaira, and N. Ueno, J. Appl. Phys. **99**, 093705 (2006).
[34]T. Sueyoshi, H. Kakuta, M. Ono, K. Sakamoto, S. Kera, and N. Ueno, Appl. Phys. Lett. **96**, 093303 (2010).

[35]S. Wang, T. Sakurai, R. Kuroda, and K. Akimoto, Appl. Phys. Lett. **100**, 243301 (2012).
[36]W. Brütting, S. Berleb, and A. G. Mückl, Org. Electron. **2**, 1 (2001).
[37]K. Schulze, C. Uhrich, R. Schuppel, K. Leo, M. Pfeiffer, E. Brier, E. Reinold, and P. Bauerle, Adv. Mater. **18**, 2872 (2006).
[38]J. Wagner, M. Gruber, A. Wilke, Y. Tanaka, K. Topczak, A. Steindamm, U. Hörmann, A. Opitz, Y. Nakayama, H. Ishii, J. Pflaum, N. Koch, and W. Brütting, J. Appl. Phys. **111**, 054509 (2012).
[39]Y. Noguchi, Y. Tanaka, Y. Miyazaki, N. Sato, Y. Nakayama, and H. Ishii, in *Physics of Organic Semiconductors*, edited by W. Brütting and C. Adachi (Wiley-VCH, 2012), Chap. 5.
[40]J. Takahashi and H. Tokairin, personal communication (2014).
[41]Y. Nakayama, S. Machida, Y. Miyazaki, T. Nishi, Y. Noguchi, and H. Ishii, Org. Electron. **13**, 2850 (2012).
[42]Y. Noguchi, H. Lim, T. Isoshima, E. Ito, M. Hara, W. W. Chin, J. W. Han, H. Kinjo, Y. Ozawa, Y. Nakayama, and H. Ishii, Appl. Phys. Lett. **102**, 203306 (2013).
[43]Q. L. Song, F. Y. Li, H. Yang, H. R. Wu, X. Z. Wang, W. Zhou, J. M. Zhao, X. M. Ding, C. H. Huang, and X. Y. Hou, Chem. Phys. Lett. **416**, 42 (2005).
[44]V. Tripathi, D. Datta, G. S. Samal, A. Awasthi, and S. Kumar, J. Non-Cryst. Solids **354**, 2901 (2008).